Field-dependent magnetic and transport properties and anisotropic magnetoresistance in ceramic $La_{0.67}Pb_{0.33}MnO_3$

1999 J. Phys.: Condens. Matter 11 8111

(http://iopscience.iop.org/0953-8984/11/41/314)

J. Phys.: Condens. Matter **11** (1999) 8111–8130. Printed in the UK PII: S0953-8984(99)05378-3

Field-dependent magnetic and transport properties and anisotropic magnetoresistance in ceramic $La_{0.67}Pb_{0.33}MnO_3$

A Peles, H P Kunkel, X Z Zhou and Gwyn Williams

Department of Physics and Astronomy, University of Manitoba, Winnipeg R3T 2N2, Canada

Received 22 June 1999

Abstract. A summary of detailed measurements of the field and temperature dependence of the ac susceptibility, magnetization and the longitudinal and transverse magnetoresistivities of ceramic $La_{0.67}Pb_{0.33}MnO_3$ is presented. Detailed analysis of the magnetic data provides an estimate of 340.5 ± 0.5 K for the paramagnetic to ferromagnetic transition temperature T_c, with the data closest to the critical point yielding $\gamma = 1.39 \pm 0.06$ (from the temperature dependence of the susceptibility along the crossover line), $\beta = 0.41 \pm 0.02$ (from the field induced variation of the temperature of the same line) and $\delta = 4.20 \pm 0.15$ (from the field dependence of the critical isotherm). Nevertheless the presence of disorder—a variance in the distribution of spin–spin coupling strengths—means that Heisenberg model (asymptotic) exponents cannot be excluded; the universality class for this system cannot therefore be definitively identified.

The transport data yield $T_c = 339.6 \pm 0.4$ K, and while the isotropic magnetoresistance peaks near T_c, as expected, the magnitude of the spontaneous resistive anisotropy (SRA) (the difference between the longitudinal and transverse magnetoresistance extrapolated to zero induction) increases linearly with decreasing temperature below T_c, peaks near 30 K and then falls to a smaller value ($-0.2 \pm 0.03\%$) in the liquid helium range. While this latter value is in reasonable agreement with itinerant model predictions, the temperature variation in the SRA above 30 K is more convincingly reproduced by a localized model. Furthermore, the mechanisms controlling the isotropic magnetoresistance and the SRA in this system appear to be different.

1. Introduction

Much recent research effort has been directed at understanding the magnetic and transport properties of doped lanthanum manganites, $La_{1-x}A_xMnO_3$ (A = Ca, Sr, Ba, Pb etc), and the interplay between magnetic order and the conduction process in them [1]. This interest has both a fundamental and an applied perspective. In terms of the latter these systems may have several potential applications; in particular near $x \sim 0.3$ these systems behave as half-metallic ferromagnets in which the conduction process is accomplished within a completely spin polarized band [2], thus raising the possibility of fabricating devices based on spin—rather than charge—transport. These perovskites also provide interesting possibilities for studying the fundamental behaviour of strongly correlated electronic systems. While the parent compound ($x = 0$) is a layered antiferromagnetic insulator, the substitutional replacement of trivalent La ions by divalent alkaline earths of the type indicated above produces an inhomogeneous distribution of mixed valent Mn^{3+}–Mn^{4+} ions to maintain charge neutrality and a modification of both the magnetic and the transport properties. Current models for the transport properties of the substituted systems suggest that for $x \gtrsim 0.1$ the $e_g(\Gamma_3)$ electrons at trivalent Mn sites acquire mobility (presumably due to the emergence of an e_g–$O(2p_\sigma)$ band near this composition) resulting in metallic features ($d\rho/dT > 0$) at low [1] temperature, although a few cases of

0953-8984/99/418111+20$30.00

metallic conduction at high temperatures have also been observed [3]. Of particular importance in the transport behaviour is the presence of double exchange [4], the principal consequence of which is to inhibit the hopping of electrons between Mn near-neighbour mixed valent sites when the associated quasi-localized $t_{2g}(\Gamma_5)$ core spins are not parallel. The establishment of ferromagnetic order thus enhances the conductivity substantially (the kinetic energy change of the carriers being stabilized by the ordering of the core spins), with the field dependence of the ordering process leading to a colossal magnetoresistance (CMR) near the ordering temperature T_c.

Much recent work on these doped perovskites has concentrated on Ca substitution. This has resulted in the publication of a comprehensive phase diagram for this system [5], which exhibits rich structure as a function of both Ca composition x and temperature T. Indeed, the term 'optimal doping' was first applied to this system, a consequence of the ferromagnetic ordering temperature T_c peaking (at about 250 K) close to $x \simeq \frac{1}{3}$. Here we report measurements on a ceramic sample doped with Pb at $x \simeq \frac{1}{3}$; these measurements include field-and temperature-dependent magnetic and transport measurements as well as anisotropic magnetoresistance studies. The results of such measurements are discussed below.

2. Experimental details

Samples of $La_{0.67}Pb_{0.33}MnO_3$ (nominal) were prepared by standard ceramic techniques. Stoichiometric quantities of La_2O_3 (ultra-pure), PbO and MnO_2 were mixed for 24 hours by ball milling in acetone. The dried powder was subsequently pressed into pellet form and heated to 800 °C for 24 hours; this was repeated three times following intermediate 6 hour periods of ball milling. The powder was then mixed with a binder, pressed into pellet form and annealed at 1100 °C in air for 72 hours, followed by 20 hours at 1000 °C. After removal from the furnace—effectively a quench in air—samples were treated finally for 72 hours at 600 °C. Room temperature x-ray diffraction studies of the final sample revealed a single phase, nearly cubic structure with $a = 3.8927$ Å and a slight rhombohedral distortion, $\beta = 90.30°$. These structural features correlate well with the relatively high paramagnetic to ferromagnetic and metal–insulator transition temperatures (reported below) for this system as shown by a recent bond-valence analysis of such effects in the manganese perovskites [6].

Transport and magnetic measurements were performed on the same specimen with approximate dimensions $(6 \times 1 \times 1)$ mm^3. Ac susceptibility and dc magnetization data were acquired as a function of both field and temperature using a Quantum Design PPMS model 6000 magnetometer/susceptometer. Resistance and magnetoresistance measurements were carried out using a conventional four-probe method using both standard dc (77–380 K) and a previously described low frequency (37 Hz) ac technique [7] (1.7–30 K); in both methods the measuring current flowed along the largest sample dimension.

3. Results and discussion

3.1. Zero-field resistivity

Figure 1 reproduces the temperature dependence of the zero-field resistivity $\rho(T)$ of this polycrystalline ceramic specimen between 1.7 and 380 K. These data are in good overall agreement with existing measurements on this system [8], so little comment on them is necessary. This specimen displays semiconducting behaviour ($d\rho/dT < 0$) above 350 K, the latter being the temperature of the resistivity maximum, below which an abrupt transition to metallic-like transport ($d\rho/dT > 0$) occurs. The weak, broad 'shoulder' between 150 and

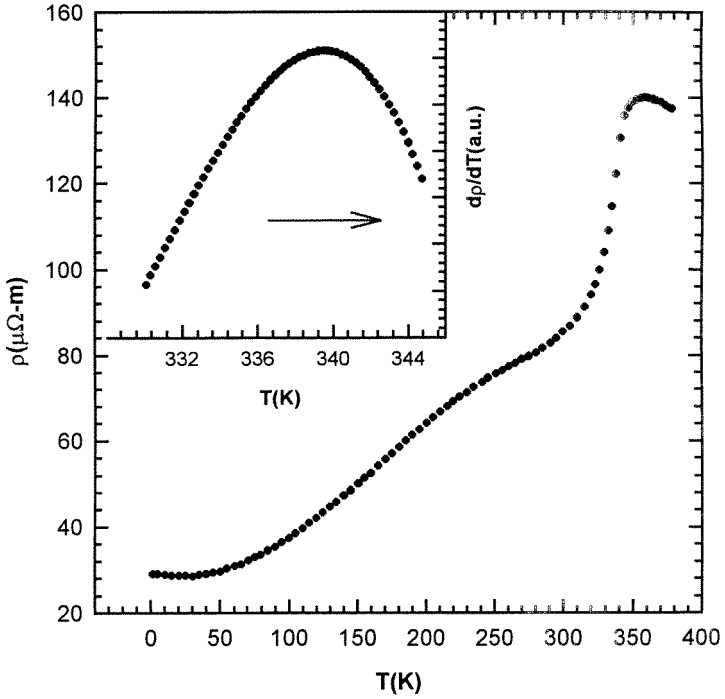

Figure 1. The zero-field resistivity ρ (in $\mu\Omega$ m) plotted against temperature (in K); the inset shows the derivative $\mathrm{d}\rho/\mathrm{d}T$ (in arbitrary units) in the vicinity of the metal–insulator transition.

300 K is attributable to sample granularity [9, 10]. The insert in this figure shows the derivative of these data in the temperature range 330–345 K, an interval that brackets the onset of the metal–insulator transition. This derivative can be seen to peak at 339.6 ± 0.4 K, a feature discussed in more detail below.

3.2. Magnetization and ac susceptibility

The inset in figure 2 shows the zero-field ac susceptibility $\chi_0(T)$ (measured at 2.4 kHz with a driving field amplitude of 3 μT) of the same specimen; $\chi_0(T)$ increases rapidly as the temperature is lowered and the system passes through the metal–insulator transition. The zero-field susceptibility exhibits a maximum near 320 K (the Hopkinson peak [11]) before decreasing slowly with further decrease in temperature.

The detailed behaviour of this magnetic response is presented in the main body of this figure. Here the effects of static biasing fields of 30–100 mT superimposed on the ac field are shown (both ac and dc fields being applied parallel to the largest sample dimension). As has been reported in a variety of other systems, both metallic and semiconducting [12], such static fields suppress the principal maximum in both amplitude and temperature, enabling the critical peaks evident in the main body of this figure to be resolved. These critical (secondary) maxima decrease in amplitude and move upward in temperature as the static biasing field H_a increases, a behaviour which—as discussed in detail previously [12]—is characteristic of critical fluctuations in the vicinity of a continuous magnetic phase transition. The result that the temperatures T_m of these critical maxima move upward, while their amplitude $\chi(H, T_m)$ decreases with increasing field H, is consistent not only with the general formalism based on

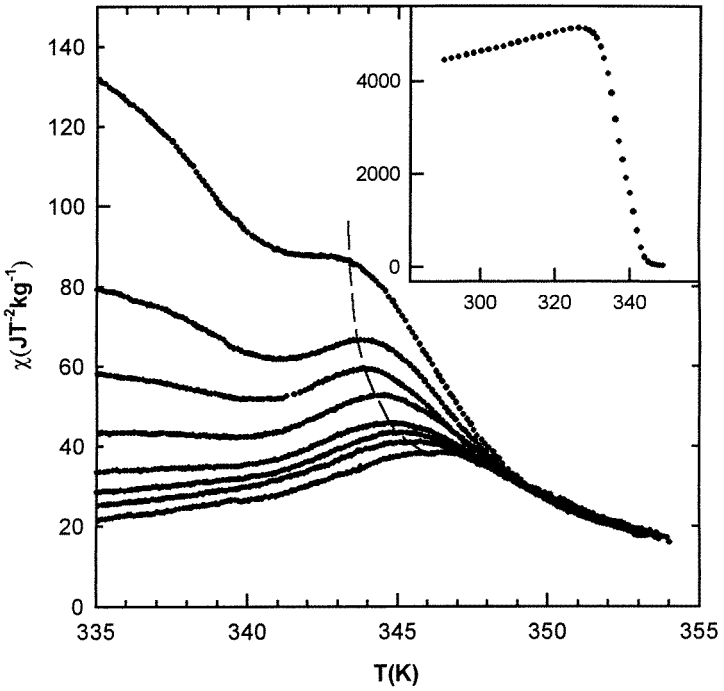

Figure 2. The temperature dependence of the ac susceptibility χ (in J T^{-2} kg^{-1}) plotted against temperature (in K) in the vicinity of the paramagnetic to ferromagnetic transition. The inset shows the zero-field ac susceptibility while the data in the main figure were taken in static biasing fields $\mu_0 H_a$ of between 30 and 100 mT increasing (from top to bottom) in steps of 10 mT. The dashed line designates the cross-over line (see text).

the static scaling law description of such a transition [13], but also with detailed numerical solution of a particular model—the ferromagnetic phase of a Sherrington–Kirkpatrick-like (S–K) model [14] (within the latter this peak evolution is consistent—as expected—with mean field exponent values). The fluctuation–dissipation theorem provides a qualitative understanding of the emergence of such peaks in finite field [15], and also indicates that the locus of these critical maxima delineates the location of the 'cross-over' line in the (H–T) plane, above which the susceptibility is dominated by thermal fluctuation whereas below this line it is field dominated.

A quantitative analysis of these data is based on the conventional static scaling law equation of state which expresses the (reduced) magnetization m in terms of the usual linear scaling fields $h \sim H_i/T_c$ and $t = |T - T_c|/T_c$, where H_i is the internal field and T_c the critical (ferromagnetic) temperature, i.e.

$$m = t^{\beta} F(h/t^{\gamma+\beta}). \tag{1}$$

Alternatively

$$\chi(h,t) = \frac{\partial m}{\partial h} = t^{-\gamma} G\left(\frac{h}{t^{\gamma+\beta}}\right) = h^{1-1/\delta} H\left(\frac{h}{t^{\gamma+\beta}}\right) \tag{2}$$

in which $H(X) = X^{\gamma/\gamma+\beta} G(X)$, where G is the derivative of the (unknown) scaling function F, and the Widom equality $\gamma = \beta(\delta - 1)$ is assumed to hold. From this latter form in equation (2) it can be seen that susceptibility measurements carried out in fixed field (for

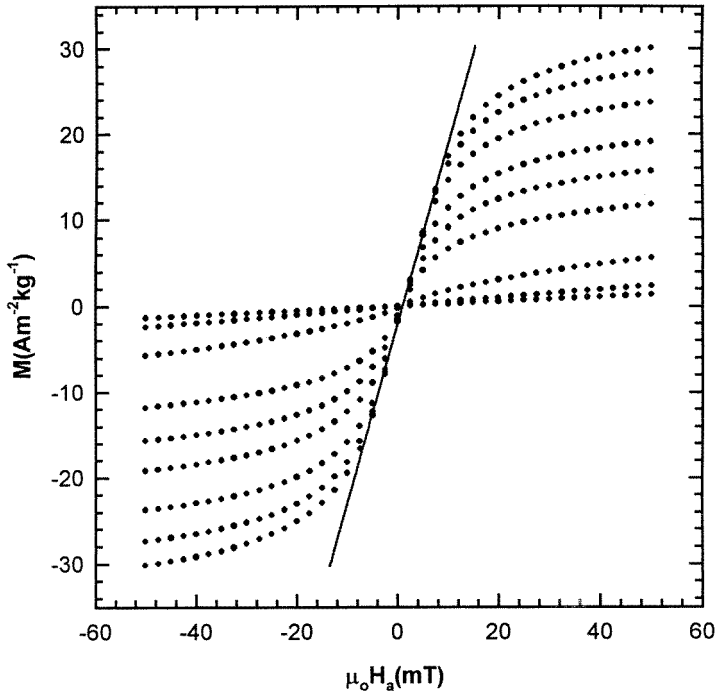

Figure 3. The magnetization M (in A m^{-2} kg^{-1}) measured in low applied fields $\mu_0 H_a$ (in mT) close to the ferromagnetic transition temperature. Here the applied field is parallel to the largest sample dimension with the solid line estimating the slope of the 'shearing' curve.

which the prefactor $h^{1-1/\delta}$ is constant) as a function of temperature map out the dependence of $H(X)$ on its argument X (in which the temperature appears in the denominator). Furthermore the assertion of scaling theory that F—and hence H and G—is a universal function of this argument means that any feature evident in $H(X)$, such as the maxima shown in figure 2, will appear at the same value (X_c) of this argument. This leads directly to

$$\frac{h}{t_m^{\gamma+\beta}} = X_C \qquad viz.\ t_m = (T_m - T_c)/T_c \propto H_i^{1/(\gamma+\beta)} \tag{3}$$

where T_m is the temperature of the maxima evident in figure 2. In addition, as the argument $X = X_c$ is a constant at these maxima, so are the functions $H(X_c)$ and $G(X_c)$ themselves, when, from the initial form in equation (2)

$$\chi(h, t_m) \propto t_m^{-\gamma}. \tag{4}$$

Thus the *peak* susceptibility displays the *same* dependence on temperature as does the zero-field susceptibility immediately above T_c. These features are exploited below as they enable various critical exponents to be deduced *directly* from these maxima, thus contrasting with estimates for γ and β, from the magnetization above and below T_c respectively, which usually involve extrapolation to zero field to avoid complications associated with contributions from the regular/non-critical components to the low field response. The approach adopted here avoids such extrapolations (and the uncertainties inherent in them) as the following demonstrates. Analysis of these data begins by plotting the peak temperatures T_m from figure 2 against $H_i^{1/(\gamma+\beta)}$; the internal field ($H_i = H_a - NM$, in the usual notation) at each temperature is estimated from the measured magnetization and the slope (N^{-1}) of the low field (shearing)

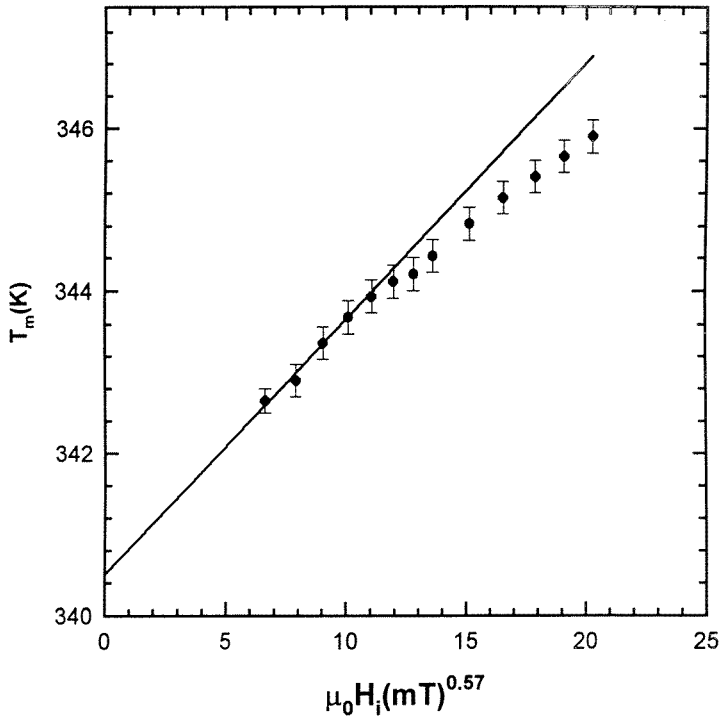

Figure 4. The ac susceptibility peak temperature T_m (in K)—taken from data similar to those shown in figure 2—plotted against $(\mu_0 H_i \text{ (in T)})^{1(\gamma+\beta)}$ where H_i is the internal field and Heisenberg model exponents are adopted ($(\gamma + \beta)^{-1} = 0.57$). The intercept of the straight line drawn yields an estimated T_c.

curve, figure 3. Such plots have been constructed using a wide range of exponent values; the most consistent 'fits'—discussed below—are obtained with values of $(\gamma + \beta)$ close to those predicted by the isotropic, nearest-neighbour three-dimensional Heisenberg model [16], *viz.* $\gamma + \beta = 1.75$, which are used in figure 4. The intercept of the straight line drawn in this figure (resulting from the fitting of the first six points, i.e. those closest to T_c, which is appropriate considering the asymptotic nature of the scaling law ($h \to 0$, $t \to 0$)), provides an estimate for T_c of 340.5 ± 0.5 K. There are deviations away from the single power-law behaviour summarized in equation (3) evident at higher fields, and a possible origin for such deviations is discussed later. At this point it is important to point out that the behaviour presented in figure 4, in particular the T_c estimate, is essentially independent of the exponent values chosen (mean field, 3D Heisenberg etc). This estimate for the ferromagnetic ordering temperature from the magnetic data is in very good agreement with that deduced above from the transport measurements (339.6 ± 0.4 K), particularly since these data sets were acquired in different cryostats incorporating different thermometry (the absolute accuracy of which is typically 0.5–1% in either system). The estimate of $T_c = 340.5$ K is then used in constructing other scaling plots from the magnetic data, as detailed below.

The susceptibility peak amplitudes from figure 2 (corrected for background and demagnetizing effects) are plotted against the reduced temperature t on a double logarithmic scale in figure 5. The straight line drawn in this figure—a best fit to the 11 points (those approaching the asymptotic limit most closely)—verifies the power-law prediction of equation (4), with the slope of this line yielding $\gamma = 1.39$. This value is in close agreement

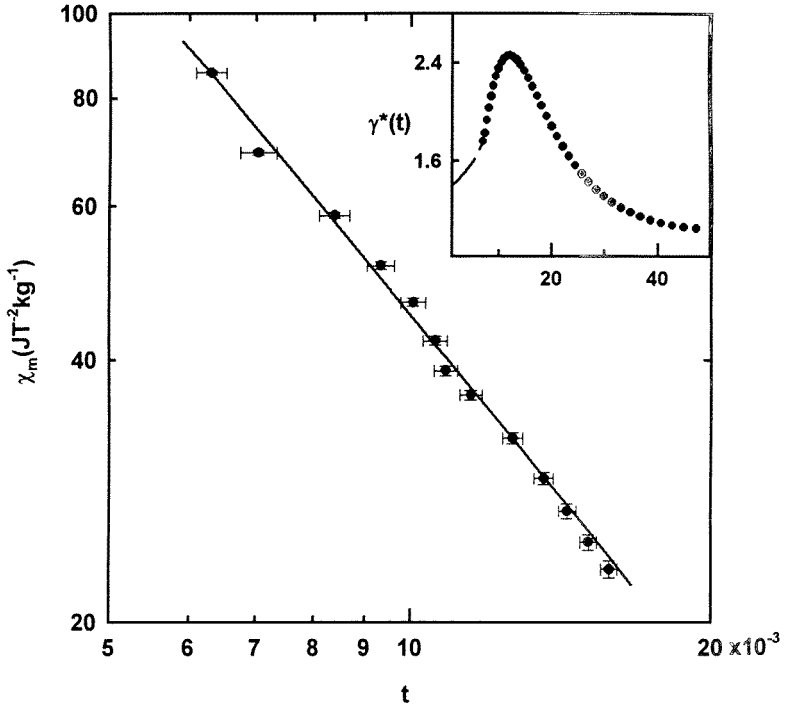

Figure 5. The field-dependent ac susceptibility peak amplitude χ_m (in J T^{-2} kg^{-1})—taken from data similar to those shown in figure 2—and plotted against the reduced peak temperature t_m on a double logarithmic scale. The slope of the line drawn not only confirms the power-law prediction of equation (4) but also yields $\gamma = 1.39$. The inset shows the behaviour of the effective Kouvel–Fisher (zero-field) susceptibility exponent $\gamma^*(t)$ (see text).

with the three-dimensional Heisenberg model prediction of 1.386, a result that provided a principal impetus for investigating overall consistency with this latter model exponent values. With the uncertainties evident in figure 5, the range of slopes that will fit these data yields

$$\gamma = 1.39 \pm 0.06.$$

Figure 6 assesses the applicability of Heisenberg model exponents in describing the field induced increase in the temperature of the crossover line, *viz*. a double logarithmic plot of the reduced peak temperature t_m from figure 2 against the internal field H_i. An unrestricted best fit to the initial five points in this figure yields $(\gamma + \beta)^{-1} = 0.54$, somewhat lower than the Heisenberg model value of 0.57 actually shown in this figure. The latter provides an acceptable fit, although deviations are clearly evident at higher field (so that fitting the entire data set would clearly reduce the estimate for $(\gamma + \beta)^{-1}$). Having decided to investigate the overall applicability of Heisenberg model exponents, it is appropriate to discuss possible causes of deviations from these model values evident in figure 6 at higher fields. Indeed, close examination of figure 5 indicates an increase in slope (and hence in the effective susceptibility $\gamma^*(t)$ defined below) beyond $t \simeq 5 \times 10^{-3}$, while the data in figure 6 display marked (concave) curvature above $t_m \sim 10^{-2}$ consistent with an increase in the sum of the corresponding effective exponents $(\gamma^* + \beta^*)$ beyond that point. *Effective* exponent values defined, for example, through the Kouvel–Fisher expressions [17].

$$\gamma^*(t) = \mathrm{d}(\ln \chi(0,t))/\mathrm{d}\ln(t) \qquad \beta^*(t) = \mathrm{d}(\ln m(0,t))/\mathrm{d}\ln(t)$$

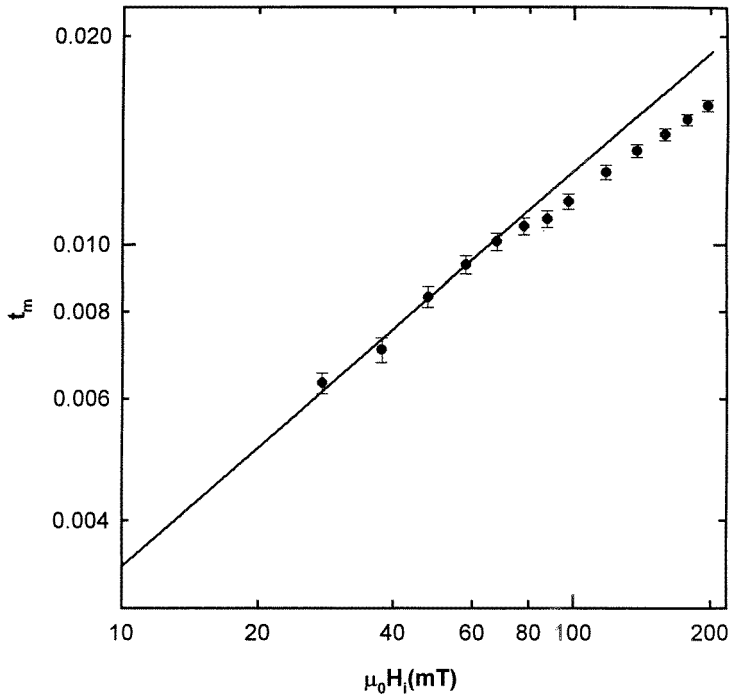

Figure 6. The field-dependent ac susceptibility reduced peak temperature t_m plotted against the internal field $\mu_0 H_i$ (in mT) on a double logarithmic scale. The straight line drawn corresponds to the power-law prediction of equation (3) with Heisenberg model exponents.

which change with increasing temperature or field are an established feature of coupled spin systems in which the spin–spin (exchange) coupling constants displays some variance about a mean value. The effective Kouvel–Fisher susceptibility exponent $\gamma^*(t)$ derived from the present zero-field data is shown in the inset in figure 5. In this regard, the consensus emerging from previous investigations of metallic systems with such characteristics [12, 18] indicates that the 'disorder'—measured typically by the variance in the distribution of coupling strengths—is an irrelevant scaling field *at* the critical point ($t = 0$, $h = 0$), so that the asymptotic exponent values are unchanged from the 'pure' system in agreement with the Harris criterion (as the specific heat exponent $a < 0$). The 'disorder' does however cause the effective exponent values to change as field and/or temperature is varied away from the critical point [12, 18]. Various model calculations of such effects have been performed, and figures 7 and 8 reproduce the temperature dependence of $\beta^*(h)$ and $\delta^*(h)$ in the S–K model mentioned previously [19]. The initial increase in $\beta^*(h)$ from its asymptotic value (β_0) shown in figure 7 is qualitatively consistent with the behaviour of the data reproduced in figure 6; such calculations thus reproduce correctly the *trends* observed experimentally, although the mean-field nature of the S–K model cannot reproduce the correct asymptotic *value* for β_0 (0.5 in the S–K model, cf 0.365 in the Heisenberg model). It should also be noted that these calculations utilize a Gaussian distribution of exchange coupling constants (with $\eta = J_0/J$ being the ratio of the first to second moment of the distribution), whereas that characterizing the present system is probably bimodal: a dominant ferromagnetic component arising from double exchange between Mn^{3+} and Mn^{4+} ions and an antiferromagnetic component resulting from Mn^{3+}–Mn^{3+} interactions (so called t_{2g}–$O(2p_\pi)$–t_{2g} superexchange) prevalent in the undoped host, each

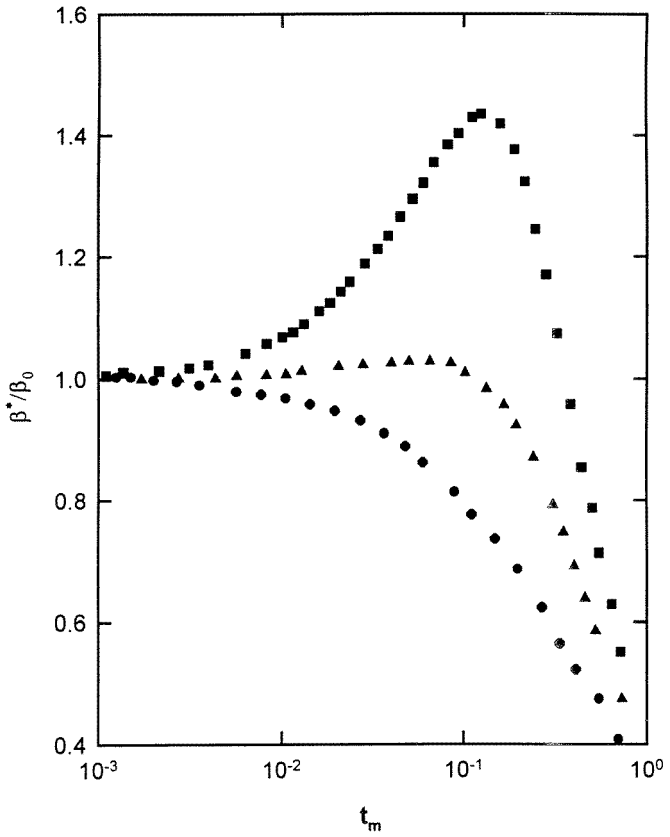

Figure 7. The ratio of the effective Kouvel–Fisher exponent β^* to its asymptotic value β_0 calculated from the ferromagnetic phase of an S–K-like model (see text), plotted against the reduced susceptibility peak temperature t_m. The symbols correspond to (■) $\eta = 1.27$, (▲) $\eta = 2$, (●) $\eta = \infty$.

weighted appropriately by the proportion of Mn^{3+} and Mn^{4+} ions present, i.e. the doping level. Available calculations [20] suggest that differences in the distribution profiles should not influence significantly the trends described above. The mean-field nature of the S–K model, in which $\gamma(T) = \gamma^*(T)$, cannot reproduce the trends evident in the inset in figure 5 for $\gamma^*(T)$, although other approaches incorporating exchange coupling disorder have been invoked [21]. The final comparison involves the exponent δ. Figure 9 reproduces magnetization data acquired along the critical isotherm and plotted on a double logarithmic scale against the internal field. The straight line drawn confirms the power-law prediction of equation (1) for this isotherm, *viz.*

$$m \propto H_i^{1/\delta} \tag{5}$$

with the slope of the line drawn corresponding to $\delta = 4.2(\pm 0.15)$ for $20 \leqslant H_i \leqslant 10^3$ mT. The latter is well below the three-dimensional Heisenberg model value of 4.80.

The analysis of the magnetic data given above thus admits the following alternatives.

A best fit to data closest to the critical point ($t = 0$, $h = 0$) yields

$$\gamma = 1.39 \pm 0.06 \qquad \beta = 0.41 \pm 0.02 \qquad \delta = 4.2 \pm 0.15.$$

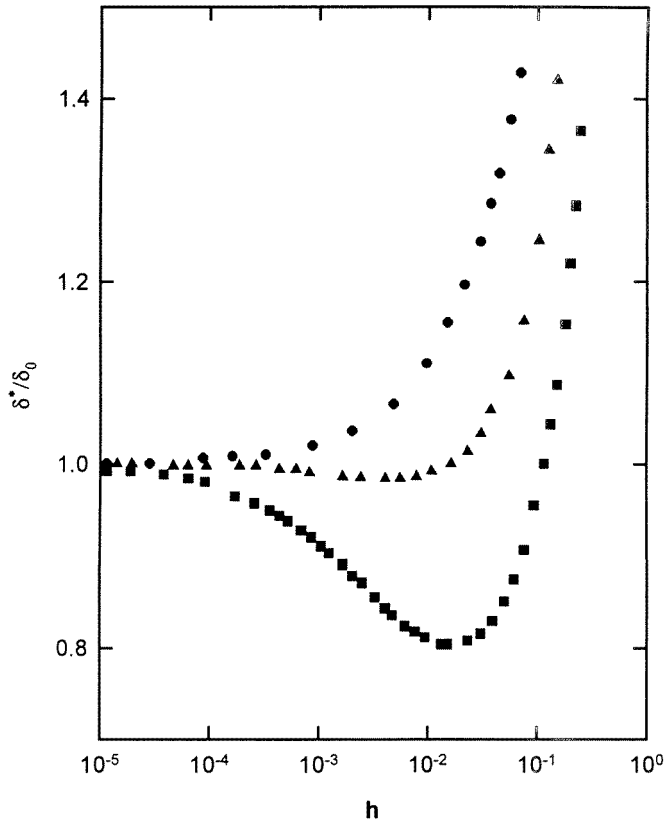

Figure 8. The ratio of the effective exponent δ^* to its asymptotic value δ_0 calculated from the local slope of the critical isotherm at the ferromagnetic boundary in an S–K-like model (see text); symbols as in figure 7.

These estimates satisfy the Widom equality

$$\gamma = \beta(\delta - 1)$$

within experimental uncertainty ($\delta - 1 - \gamma/\beta = 0.2 \pm 0.27$); however they do not agree with the predictions of any specific model. Nevertheless the estimates for δ and β agree, again within the listed uncertainty, with the corresponding estimates reported recently [22] for single crystal $La_{0.7}Sr_{0.3}MnO_3$ ($\delta = 4.25 \pm 0.2$, $\beta = 0.37 \pm 0.04$), although the estimate for γ in that system (1.22 ± 0.03) is lower than that found here.

Alternatively arguments incorporating the effects of exchange bond disorder—which, as outlined above, appear to suggest that the *asymptotic* estimates for γ and β in the present system might be compatible with Heisenberg model predictions—could be extended to δ value estimates. Specifically, as depicted in figure 8, the effects of 'disorder' depress the estimate for this exponent below its true asymptotic value for data acquired away from the critical point, $h = 0$. A reduction in the effective δ^* value of some 13% from its (assumed) asymptotic value would reproduce the measured value, and while this reduction is considerable the model calculations reproduced in figure 8 show that this is achievable for $\eta \sim 1.3$ in the fields utilized here ($h = g\mu_B H_i / k_B T_c$). It is, furthermore, not inconsistent with the variation displayed by the other effective exponents.

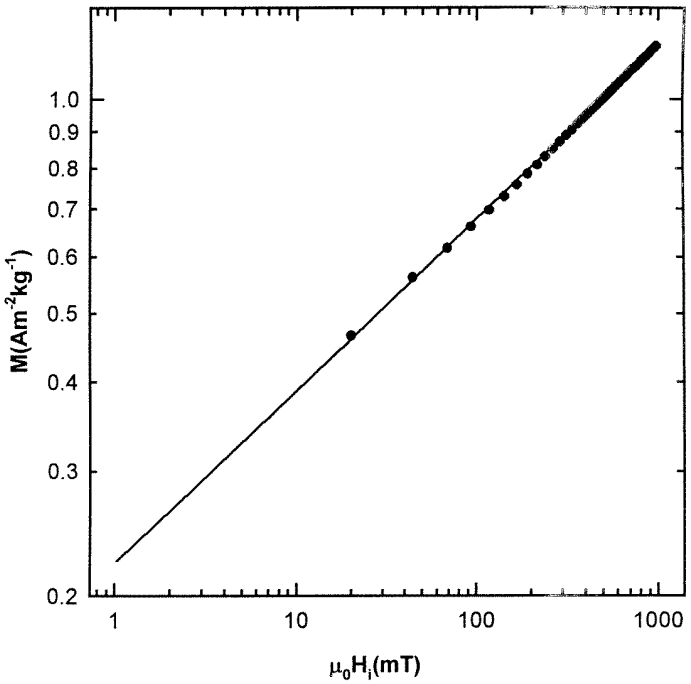

Figure 9. The magnetization M (in A m^{-2} kg^{-1}) measured along the critical isotherm, plotted against the internal field $\mu_0 H_i$ (in mT) on a double logarithmic scale. The slope of the line drawn yields $\delta = 4.2$.

In summary, both of the above suggestions must remain as possible explanations of the magnetic response of this Pb doped manganite. This situation could be resolved, in principle, by measurements closer to the critical point. Such measurements are, however, precluded by the presence of a significant regular (i.e. noncritical) contribution to the response which obscures the emerging critical peak structure (and hence the critical response) as is clearly apparent in figure 2. This latter behaviour is a somewhat ubiquitous feature of doped perovskites. In many non-perovskite systems previously studied, the presence of such a regular component, which is not driven to (technical) saturation in relatively low fields, has been associated with an anisotropy/coercivity arising from single ion spin–orbit coupling [12, 23]. The coercivity of the present sample—obtained from butterfly loop measurements ($\chi(H_a, T)$ against H_a at various fixed temperatures)—is shown as a function of temperature in figure 10. $H_c(T)$ collapses to zero near $T_c \simeq 340$ K, as shown in the inset in this figure, and saturates at a value of about 1.6 mT below 250 K, somewhat lower than that reported recently for similarly prepared ceramic $La_{0.67}Ca_{0.33}MnO_3$ bulk samples [24], and roughly an order of magnitude lower than LCMO films [25]. It would be tempting to attribute this coercivity to the presence of Mn^{3+} ions (Mn^{4+} is not a Jahn–Teller ion), a corollary of which would be that this system should also display a spontaneous resistive anisotropy, already reported for the other divalent dopants, and which is considered in the following section.

3.3. Magnetoresistance and the spontaneous resistive anisotropy (SRA)

Having briefly discussed the zero-field transport data (figure 1) earlier, the detailed behaviour of the effects of an external magnetic field is now presented. Figure 11 displays the longitudinal

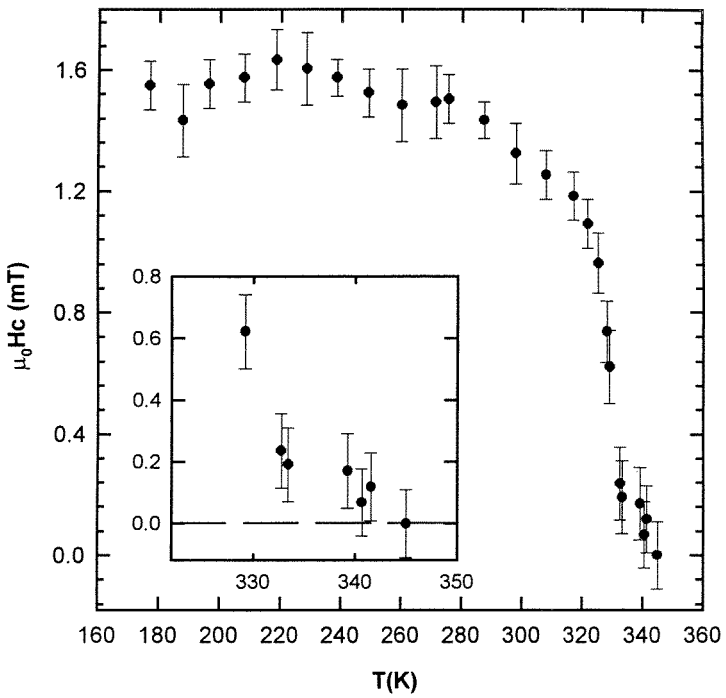

Figure 10. The coercive field $\mu_0 H_c$ (in mT), estimated from butterfly-loop measurements, plotted against temperature (in K). The inset shows the behaviour close to the ferromagnetic transition temperature T_c.

$\rho_\parallel$ (H_a parallel to the measuring current) and the transverse $\rho_\perp$ magnetoresistance at 4.2 K in fields up to 3 T. In both orientations the low field magnetoresistance ($\mu_0 H_a < 0.5$ T) falls sharply, as shown in the inset, an effect often attributed to grain boundary effects [25], with the large difference evident between the two orientations originating principally from demagnetizing field effects (estimated to be about $\leqslant 0.2$ T), as discussed below). At higher fields ($\gtrsim 1$ T) there is a much slower, essentially linear decrease in $\rho(H_a)$ with increasing applied field H_a.

The spontaneous resistive anisotropy (SRA) is usually defined by the ratio [26]

$$\frac{\Delta\rho}{\rho_0} = \left[\frac{\rho_\parallel(B) - \rho_\perp(B)}{\rho_0}\right]_{B\to 0} \tag{6}$$

which characterizes the difference between the longitudinal and transverse magnetoresistance of a (technically) single domain ferromagnet extrapolated to zero induction, roughly the transport equivalent of the spontaneous magnetization. The extrapolation implicit in equation (6) is usually performed from a field region sufficiently high to (technically) saturate the sample; by contrast the low field region of the curves shown in the inset in figure 11 depend on the prevailing domain structure which is, in turn, history dependent and hence not well defined [27]. The extrapolations, shown by the dashed lines in this figure, are fits to the (technically saturated) data beyond $\mu_0 H_a \sim 1$ T where a simple linear, essentially parallel, fit reproduces the data for both orientations very well. These extrapolations are extended to $B = 0$, where $B = \mu_0 H_a + M(\mu_0 - N)$ in the usual notation and the demagnetizing factors are found from the corresponding 'shearing' curves. For the two orientations, the difference in these latter factors results in the condition $B = 0$ being attained in applied

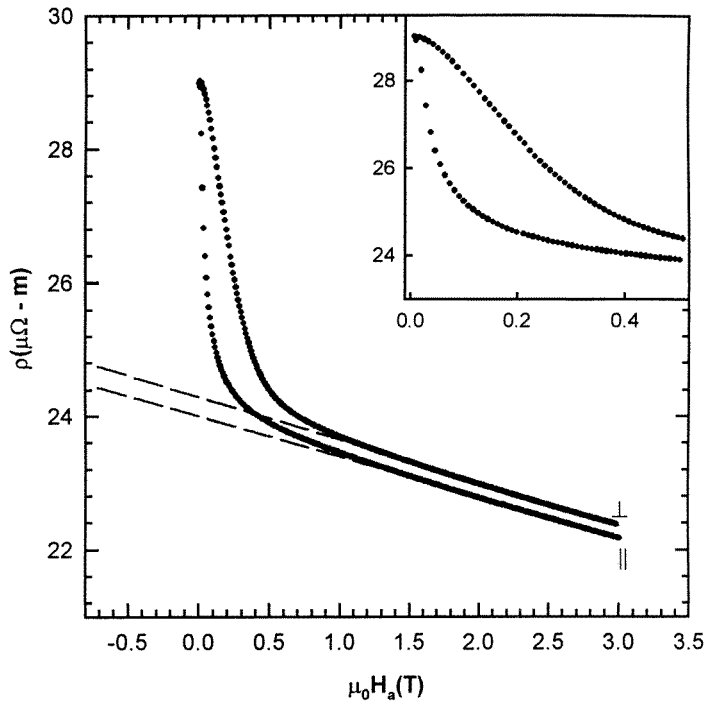

Figure 11. The resistivity ρ (in $\mu\Omega$ m), measured in the transverse ($\perp$) and longitudinal ($\parallel$) configurations at 4.2 K, plotted against the applied field $\mu_0 H_a$ (in T). The dashed lines are linear extrapolations from the high field region. The inset shows the low field behaviour in more detail.

fields $\mu_0 H_a$ differing by the $\sim$0.2 T mentioned above. The value estimated for the SRA at 4.2 K using this approach is $-0.2(1) \pm 0.03\%$. Since a non-vanishing SRA requires both a polarizing field and spin–orbit coupling at scattering sites in either an itinerant [27, 28] or a localized model approach [27, 29], this result is qualitatively consistent with the presence of Mn^{3+} ions mentioned above. Both the sign and magnitude of this effect in the Pb substituted system is similar to that reported for expitaxial films of $La_{0.67}Sr_{0.33}MnO_3$ films at the same temperature [30] and for post-annealed films of $La_{0.7}Ca_{0.3}MnO_3$ on $SrTiO_3$ at higher temperatures [25].

Before discussing both the size and the temperature dependence of the SRA in this substituted perovskite, two further comments on the behaviour evident in figure 11 are appropriate. First, in metallic ferromagnets the change in $\rho_\perp$ or $\rho_\parallel$ with applied field beyond technical saturation is usually attributed to Lorentz force considerations resulting in cyclotron curvature effects. The latter causes $\rho_\parallel$ and $\rho_\perp$ to increase with field whereas the opposite trend is evident here; furthermore cyclotron curvatures effects are generally very small in the present field range for residual resistivities greater than 10^{-2}–10^{-1} $\mu\Omega$ m [26]. The decrease in the magnetoresistivities beyond $\mu_0 H_a \sim 1$ T evident in figure 11 probably arise from some degree of non-collinearity in the spin system, as confirmed qualitatively by the corresponding magnetization data (figure 12). Quantitatively however, the fractional change in the magnetoresistance between 1 and 3 T is nearly an order of magnitude larger than the corresponding magnetization change. Second, the low field magnetoresistive behaviour reproduced in the inset in figure 11 indicates that while the behaviour evident in this regime indicates a clear anisotropy in this response, a quantitative characterization of effects

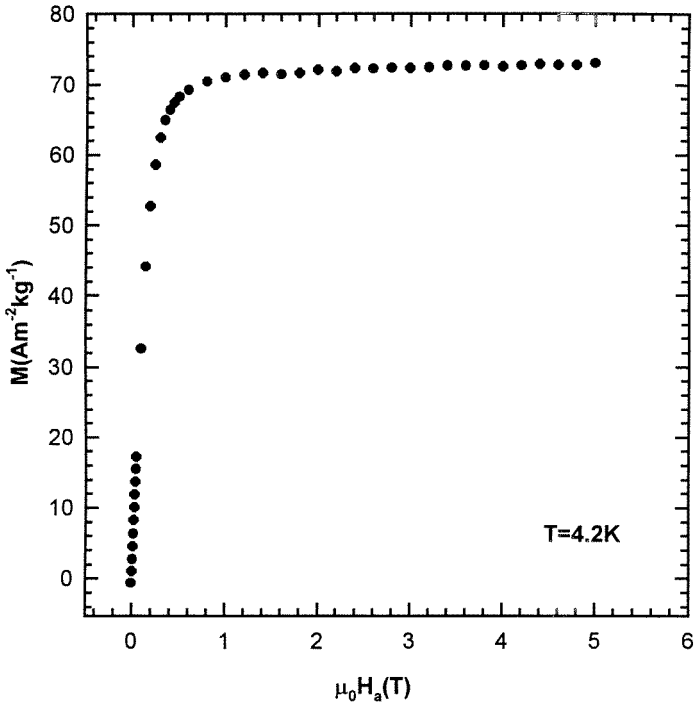

Figure 12. The magnetization M (in A m^{-2} kg^{-1}) measured at 4.2 K, plotted against the applied field $\mu_0 H_a$ (in T) with the latter applied parallel to the largest sample dimension.

from such data might be misleading since they can appear exaggerated by demagnetizing effects.

Figures 13 and 14 show selected curves of the magnetoresistivities at a variety of temperatures between 10 and 330 K, from which the SRA has been estimated in the manner described above. These data also indicate a monotonic decrease in the *low* field magnetoresistance with increasing temperature, a feature referred to later. Figure 15 summarizes the temperature dependence of the SRA so obtained.

Such data have been interpreted using two complementary models both relying on the existence of spin–orbit coupling and a polarizing field at scattering sites, as mentioned above. One is based on an itinerant picture—the two-current model—which has been utilized widely to describe extensive sets of measurements on dilute ferromagnetic alloys based on transition metal hosts [26, 27, 28, 31]; the second uses the opposite extreme—a localized picture—and has been used principally to interpret the SRA induced in paramagnetic systems such as **Au**Ho by externally applied polarizing fields [29].

Both models have been discussed in detail previously; consequently their main predictions alone will be presented here. Indeed, a recent calculation of the SRA in an itinerant model approach incorporating conduction within a single spin-polarized $e_g^{\uparrow}$ sub-band generally believed to apply to the manganese perovskites yielded [25]

$$\frac{\Delta\rho}{\rho_0} = -\frac{3}{2}\left[\frac{\lambda^2}{(H_{ex} - \Delta_{CF})^2} - \frac{\lambda^2}{\Delta_{CF}^2}\right] \tag{7}$$

where λ is the spin–orbit coupling constant, H_{ex} the exchange field and Δ_{CF} the crystal field splitting; with the latter estimated at 2 and 1.5 eV respectively and $\lambda \simeq 4 \times 10^{-2}$ eV,

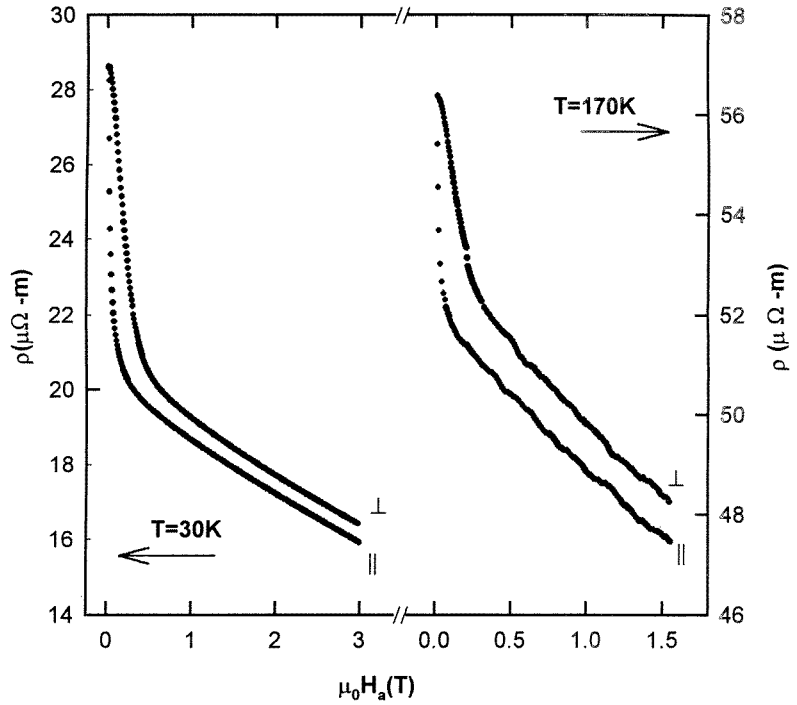

Figure 13. As in figure 11 for temperatures of 30 and 170 K.

the predicted value for the SRA is −0.85% [25]. The low temperature data displayed in figure 15 are in general agreement with this estimate—in both sign and magnitude (SRA $= -0.2(1) \pm 0.03\%$ at 4.2 K, essentially the same as at 1.5 K, but climbing abruptly to $-1.3 \pm 0.1\%$ near 30 K).

Next, the temperature dependence of the SRA is addressed. Here the *low* temperature anisotropy is an intraband effect, that is, it arises from the diagonal term ($\lambda L_z S_z$) in the spin–orbit interaction ($\lambda \vec{L}\vec{S} = \lambda L_z S_z + \lambda/2(L^+S^- + L^-S^+)$). The off-diagonal terms involve coupling to the $e_g^{\downarrow}$ sub-band; such process are inelastic (the manganese perovskites are 'strong' ferromagnets) and are frozen out at low temperature. However with increasing temperature some thermal occupation of the $e_g^{\downarrow}$ sub-band probably occurs, particularly as T_c is approached from below and the exchange splitting between spin-up (with resistivity $\rho_{\uparrow}$) and spin-down ($\rho_{\downarrow}$) sub-bands collapses. Furthermore, close to T_c an expansion of these sub-band resistivities in terms of the exchange field H_{ex} leads to [32]

$$\rho_{\uparrow}\rho_{\downarrow} \simeq \rho(0) \pm sH_{ex} \ldots \tag{8}$$

where s is the derivative of the sub-band resistivity with respect to the exchange field, and the profile of both sub-bands has been taken to be similar *close* to T_c. With s being determined primarily by the slope of the corresponding density of states near the Fermi energy E_F, $(\mathrm{d}N/\mathrm{d}E)_{E_F}$,

$$\frac{\Delta\rho}{\rho} \sim \frac{(\lambda/\Delta_{CF})^2(\mathrm{d}N/\mathrm{d}E)^2_{E_F}H^2_{ex}}{\rho_{\uparrow}\rho_{\downarrow} + \rho_{\uparrow\downarrow}(\rho_{\uparrow} + \rho_{\downarrow})} \tag{9}$$

in which $\rho_{\uparrow\downarrow}$ represents spin-flip scattering between the two sub-bands. Using collective electron (band) theory in which the thermal average of the magnetization $\langle M\rangle_T$ is proportional

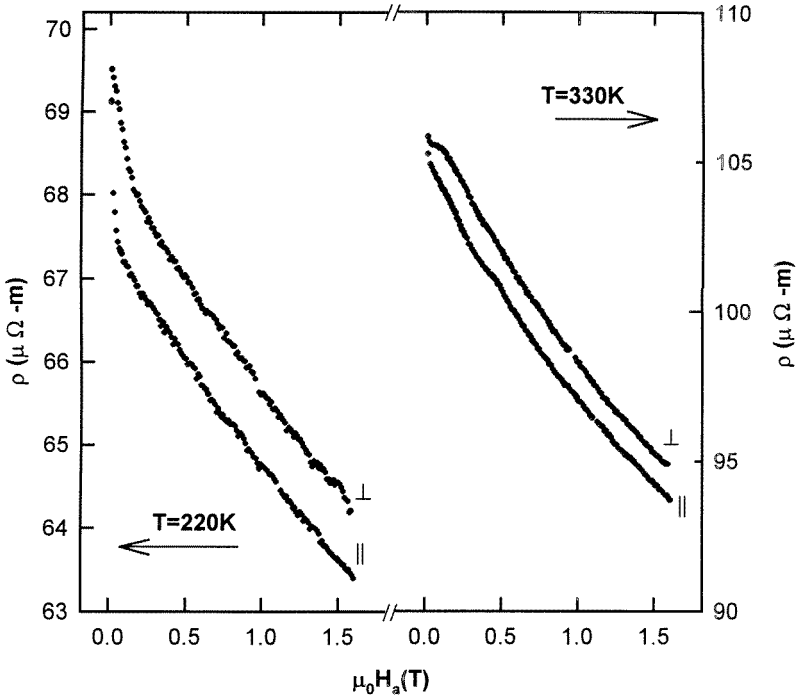

Figure 14. As in figure 13 for temperatures of 220 and 330 K.

to $(T_c - T)^{1/2}$, then in the mean field approximation in which $H_{ex} \propto \langle M \rangle_T$, one obtains

$$\frac{\Delta\rho}{\rho} \propto \frac{(\lambda/\Delta_{CF})^2 (\mathrm{d}N/\mathrm{d}E)_{E_F}(T_c - T)}{\rho_\uparrow \rho_\downarrow + \rho_{\uparrow\downarrow}(\rho_\uparrow + \rho_\downarrow)}. \tag{10}$$

Such an expression can reproduce the essentially linear decrease in the resistive anisotropy between T_c and about 100 K, provided the spin-flip and sub-band resistivities display a weak temperature dependence in this region; this is, however, an unlikely scenario within currently accepted pictures of the conduction process in the manganese perovskites. Furthermore, while the abrupt decrease exhibited by the SRA below 50 K could be modelled, for example, by some particularly sharp feature in the density of states, such arguments—along with those given above—are obviously qualitative, and a realistic comparison between experiment and the predictions of this model would necessitate incorporating realistic band structure details into the several components of equation (10) [32].

By contrast localized models reproduce the linear temperature dependence of the resistive anisotropy immediately below T_c more directly. Briefly, in this model the polarizing field aligns the spin dipole moment ($\vec{S}$) which, through spin–orbit coupling, in turn preferentially orients the orbital component ($\vec{L}$). With $L \neq 0$, the attendant non-spherical charge distribution results in a *slightly* different (charge) scattering cross-section being experienced by itinerant electrons which constitute the current as the orientation between this current and the field are changed. The analysis is effected by performing a multipole moment expansion of this aspherical *charge* distribution, from which the asymmetry, in lowest order, results from electric quadrupole (D) scattering. The resulting anisotropy ratio is given by [29]

$$\frac{\Delta\rho}{\rho_0} \simeq \left(\frac{D}{V}\right)\left[\langle S_Z^2 \rangle - \frac{S(S+1)}{3}\right] \tag{11}$$

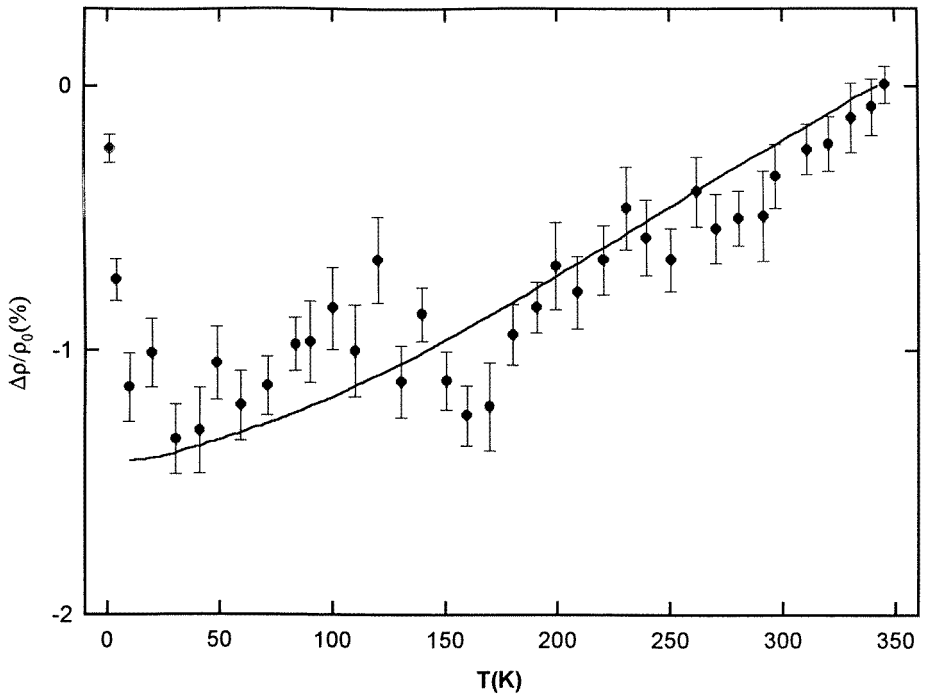

Figure 15. The temperature dependence of the estimated SRA ($\Delta\rho/\rho_0$ (%), see text). The solid line is a theoretical model prediction discussed in the text.

in which V ($\gg D$) characterizes the residual/zero-field resistivity and is usually attributed to deviations in the lattice potential from periodicity in substituted systems. Conduction band details are effectively eliminated by taking this ratio, with the quadrupole term displaying the expected $(3\cos^2\theta - 1)$ angular variation associated with axial symmetry about the field direction [27].

The solid line in figure 15 is a result of calculating $\langle S_Z^2 \rangle$ from the S–K model discussed previously [33] using $\eta = 2$ and $S = 2$; however since the calculation is scaled by the (unknown) ratio (D/V) model parameters cannot be specified from a single data set. Nevertheless this fit clearly provides a good representation of these data over the range 30 K to $T_c \simeq 340$ K using reasonable estimates for η and S. However the decrease in the magnitude of the SRA below 30 K clearly cannot be reproduced. The near linear variation in the resistive anisotropy below T_c is a feature reported in a variety of other amorphous [33] (i.e. high resistivity) and crystalline systems [32], with amorphous $Fe_{90}Zr_{10}$ also displaying a decrease in this ratio at low temperature. However, of more direct relevance is the result that the present data do *not* display a maximum in the magnitude of the SRA just below T_c where a colossal magnetoresistance is present in these systems. This result conflicts with recent reports on LCMO films, although there the anisotropy was estimated from low field data and not the extrapolation procedure utilized here.

Figure 16 summarizes the temperature dependence of the isotropic magnetoresistance measured in an applied field at 1.5 T of the same bulk ceramic $La_{0.67}Pb_{0.33}MnO_3$ as utilized in all the measurements reported here. This magnetoresistance peaks in the vicinity of T_c as expected, falls to a low value between 200 and 300 K, and then climbs monotonically with decreasing temperature to 1.5 K. If the low field decrease in the magnetoresistance

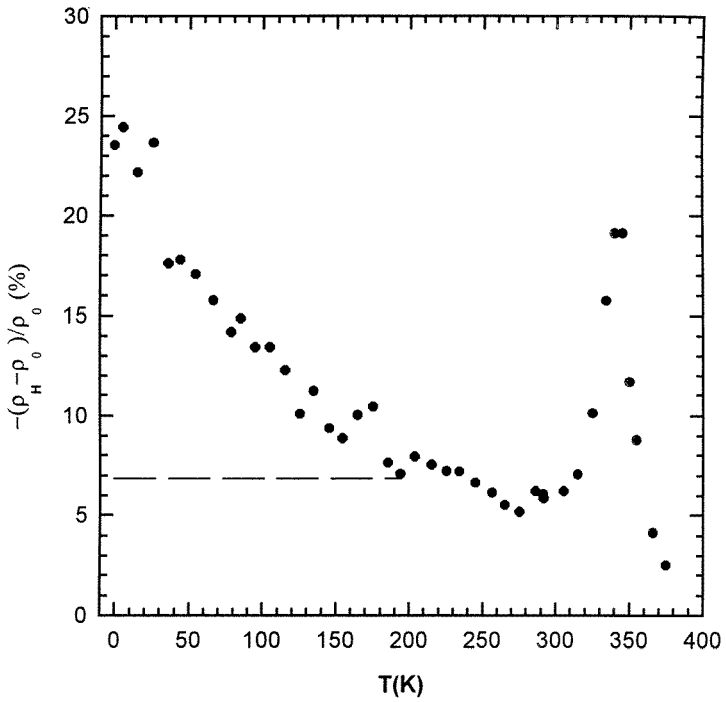

Figure 16. The temperature dependence of the isotropic magnetoresistance measured in an applied field of 1.5 T. The dashed line indicates the effect of removing the low field contribution from this ratio.

discussed previously, and attributed to grain boundary scattering, is subtracted from the data in this figure—so that only intrinsic mechanisms are considered [25]—then these data remain essentially constant below 200 K as the dashed line indicates. Since the SRA is also believed to be an intrinsic property of these systems [25], indeed the extrapolation procedure used here to estimate this quantity ensures that by removing the low field contribution, a comparison between the data in figures 15 and 16 indicates little correlation between these two effects in this Pb substituted system. An immediate conclusion that can be drawn from the latter is that the scattering mechanisms that determine the anisotropic magnetoresistance and the (isotropic) colossal magnetoresistance are not necessarily the same in all doped perovskites, a corollary of which would be that the dopant series itself—not just the presence of Mn^{3+} ions—might play some role. This possibility is currently being pursued.

4. Summary and conclusions

Field- and temperature-dependent magnetization and susceptibility measurements carried out on a ceramic $La_{0.67}Pb_{0.33}MnO_3$ sample have been analysed in an attempt to estimate the critical exponents describing the paramagnetic to ferromagnetic transition at $T_c \simeq 340$ K. Despite the detailed nature of these measurements, the universality class of this system remains uncertain. Data acquired closest to the critical point yield $\gamma = 1.39 \pm 0.06$, $\beta = 0.41 \pm 0.02$ and $\delta = 4.2 \pm 0.15$; however the presence of spin–spin coupling disorder and a significant regular component in this response admit the possibility that the asymptotic exponents might be those predicted by the three-dimensional Heisenberg model.

The spontaneous resistive anisotropy (SRA) has also been measured as a function of temperature, and, while the low temperature value for this quantity is in good agreement with recent itinerant model calculations, the linear increase in the magnitude of the SRA between T_c and about 30 K is well accounted for in a localized approach. Furthermore, the mechanisms controlling the SRA and the 'colossal magnetoresistance' appear not to be correlated here.

Acknowledgments

We would like to acknowledge the technical assistance provided by J H Zhao of this institution and the helpful discussions with Professor S H Ge, a CIDA sponsored visitor from Lanzhou University, China. We would also like to thank the Natural Sciences and Engineering Research Council (NSERC) of Canada for support of this work.

References

[1] Ramirez A P 1997 *J. Phys.: Condens. Matter* **9** 8171
Kaplan T A and Mahanti S D *Proc. Workshop on the Physics of Manganites* (New York: Plenum) at press
[2] Park J H, Vescovo E, Kim H J, Kwon C, Ramesh R and Venkatesan T 1998 *Phys. Rev. Lett.* **81** 1953
[3] Urushibara A, Moritomo Y, Arima T, Asamitsu A, Kido G and Tokura Y 1995 *Phys. Rev.* B **51** 14 103
[4] Zener C 1951 *Phys. Rev.* **82** 403
Anderson P W and Hasegawa H 1955 *Phys. Rev.* **100** 675
deGennes P G 1960 *Phys. Rev.* **118** 141
[5] Schiffer P, Ramirez A P, Bao W and Cheong S-W 1995 *Phys. Rev. Lett.* **75** 3336
Tomioka Y, Asamitsu A, Kuwahara H, Moritomo Y and Tokura Y 1996 *Phys. Rev.* B **53** R1689
[6] Rao G H, Bärner K and Brown I D 1998 *J. Phys.: Condens. Matter* **10** L757
[7] Muir W B and Ström-Olsen J O 1976 *J. Phys. E: Sci. Instrum.* **9** 163
[8] Searle C W and Wang S T 1969 *Can. J. Phys.* **47** 2703
Searle C W and Wang S T 1970 *Can. J. Phys.* **48** 2023
[9] Gupta A, Gong G Q, Xiao G, Duncombe P R, Lecoeur P, Trouilloud P, Wang Y Y, Dravid V P and Sun J Z 1996 *Phys. Rev.* B **54** R15 629
Zhang N, Ding W P, Zhong W, Xing D Y and Du Y 1997 *Phys. Rev.* B **56** 8138
[10] Zhao J H, Zhou X Z, Peles A, Ge S H, Kunkel H P and Williams G 1999 *Phys. Rev.* B **59** 8391
[11] Chikazumi S 1997 *Physics of Ferromagnetism* 2nd edn (Oxford: Clarendon) p 486
[12] Williams G 1991 *Magnetic Susceptibility of Superconductors and Other Spin Systems* ed R A Hein *et al* (New York: Plenum) p 475 *et seq*
Zhou X Z, Kunkel H P, Zhao J H, Stampe P A and Williams G 1997 *Phys. Rev.* B **56** R12 714
[13] Ho S C, Maartense I and Williams G 1981 *J. Phys. F: Met. Phys.* **11** 699
[14] Roshko R M and Williams G 1984 *J. Phys. F: Met. Phys.* **14** 703
[15] Kunkel H P, Roshko R M and Williams G 1988 *Phys. Rev.* B **37** 5880
[16] Le Guillou L C and Zinn-Justin J 1980 *Phys. Rev.* B **21** 3976
[17] Kouvel J S and Fisher M E 1964 *Phys. Rev.* A **136** 1626
[18] Kaul S N and Mohan C V 1994 *Phys. Rev.* B **50** 6157
[19] Kornik K, Kunkel H P, Roshko R M and Williams G 1990 *Solid State Commun.* **76** 993
[20] Loewen C and Roshko R M 1985 *Phys. Rev.* B **31** 4663
[21] Fähnle M 1987 *J. Magn. Magn. Mater.* **65** 1
Fähnle M and Holey T 1987 *Phys. Status Solidi* b **141** 253
[22] Ghosh K, Lobb C J, Greene R L, Karabashev S G, Shulyatev D A, Arsenov A A and Mukovskii Y 1998 *Phys. Rev. Lett.* **81** 4740
[23] Wang Z, Kunkel H P and Williams G 1990 *J. Phys.: Condens. Matter* **2** 4173
Kunkel H P, Wang Z and Williams G 1989 *J. Phys.: Condens. Matter* **1** 3381
Kunkel H P, Wang Z and Williams G 1987 *J. Phys. F: Met. Phys.* **17** L157
[24] Kumar P S A, Joy P A and Date S K 1998 *J. Phys.: Condens. Matter* **10** L487
[25] Ziese M and Sena S P 1998 *J. Phys.: Condens. Matter* **10** 2727
[26] Dorleijn J W F 1976 *Philips Res. Rep.* **31** 287

[27] Campbell I A and Fert A 1982 *Ferromagnetic Materials* vol 3, ed E P Wohlfarth (Amsterdam: North-Holland) p 747
[28] Mott N F 1936 *Proc. R. Soc.* A **153** 699
Malozemoff A 1986 *Phys. Rev.* B **34** 1853
[29] Freiderich A and Fert A 1972 *Phys. Rev. Lett.* **33** 1214
[30] Li X W, Gupta A, Gang X and Gong G Q 1997 *Appl. Phys. Lett.* **71** 1124
[31] Campbell I A, Fert A and Jaoul O 1970 *J. Phys. C: Solid State Phys.* **3** S95
[32] Stampe P A, Kunkel H P, Wang Z and Williams G 1995 *Phys. Rev.* B **35** 335
Stampe P A, Kunkel H P and Williams G 1994 *J. Phys.: Condens. Matter* **6** 3045
[33] Stampe P A, Kunkel H P and Williams G 1993 *J. Phys.: Condens. Matter* **5** L625